Kinetic and Heat Transfer Modeling of Rubber Blends' Sulfur Vulcanization with *N*-*t*-Butylbenzothiazole-sulfenamide and *N*,*N*-Di-*t*-butylbenzothiazole-sulfenamide

Blaž Likozar, Matjaž Krajnc

Faculty of Chemistry and Chemical Technology, University of Ljubljana, 1000 Ljubljana, Slovenia

Received 18 April 2006; accepted 19 July 2006
DOI 10.1002/app.25284
Published online in Wiley InterScience (www.interscience.wiley.com).

ABSTRACT: Vulcanization kinetics and heat transfer for various blends of natural (NR) and polybutadiene (BR) rubber were studied simultaneously using a mechanistic approach when developing vulcanization model kinetics. Rubber process analyzer (RPA), dynamic scanning calorimetry (DSC), and Fourier transform infrared spectroscopy (FTIR) methods were used for the study. The model reaction scheme was based on one of the best possible proposed individual reaction mechanisms. Molecular modeling was applied to distinguish between the reactivity of chemically similar species. The kinetics of *N*-*t*-butylbenzothiazole-sulfenamide (TBBS) and *N*,*N*-di-*t*-butylbenzothiazole-sulfenamide (TBSI) were treated separately using FTIR experiment data, and then incorporated in a model suitable for two-accelerator vulcanization. The proposed model quite well describes the thermal equilibration during the induction period despite a few simplifications. During cure and over-cure periods the course of vulcanization was described using a rigorous kinetic model. Physical and chemical model parameters were calculated from experimental data. Average heat transfer coefficient minimum during induction period was found to be at a weight ratio of BR and NR 1 : 1. The activation energy of significant reactions between rubber and other species was found to vary linearly with vulcanization compound composition. © 2006 Wiley Periodicals, Inc. J Appl Polym Sci 103: 293–307, 2007

Key words: modeling; kinetics; vulcanization; blends; sulfur

INTRODUCTION

A vast majority of rubber applications involve some sort of crosslinking, which is also known as the vulcanization process, most of them with addition of sulfur; sometimes, however, peroxides, amino acids, aldehydes, or some other crosslinking agents are applied. Sulfur vulcanization is the traditional yet still most common method for unsaturated elastomers. Sulfur vulcanization compound ingredients have been further developed and optimized and today sulfur is generally used alongside with a wide range of specific chemicals which provide the desired course of vulcanization and, even more importantly, preferred product properties. A standard formulation thus includes a crosslinking agent, one or more accelerators (mainly sulfur- and nitrogen-containing chemicals), activators (zinc and other metal oxides, stearic and similar fatty acids), a retarder, an antioxidant, pigments, and fillers. The complexity of formulation, however, is the main reason why the vulcanization process is still not completely understood; in particular, the mechanisms of individual reactions are still not completely known or are in dispute. Difficulties in understanding also occur due to a large number of chemically similar species, with various numbers of sulfur atoms in the polysulfidic chain, which generally react in an analogous manner; however, this should not be taken as a rule. Recent reviews of rubber crosslinking were presented. Akiba and Hashim[1] and Aprem et al.[2] reviewed the up to date literature on vulcanization and crosslinking in elastomers. Ghosh et al.[3] proposed the reaction mechanism for the different steps in vulcanization chemistry and Koenig[4] wrote a review about the chemical reactions of network structures in elastomers.

The kinetics of vulcanization have been studied in two manners. Earlier attempts were robust phenomenological approaches, which generally tended to describe the form of the vulcanization curve, but seldom tried to encompass the chemistry and the reactions during vulcanization. The macrokinetics described by phenomenological approaches are often represented by power law and other models developed by Piloyan,[5] Kamal and Sourour,[6] and Isayev and Deng.[7] All these vulcanization models more or less successfully fit the cure curve, which has the form typical for autoaccelerated reactions. However, whether two, four, or more parameters are fitted on experimental data,

Correspondence to: M. Krajnc (matjaz.krajnc@fkkt.uni-lj.si).
Contract grant sponsor: Slovenian Ministry of Higher Education, Science and Technology; contract grant number: L2-6686.

©2006 Wiley Periodicals, Inc.

they are to be compared only for similar systems giving us a relative criterion for vulcanization rates and orders in the systems in question. These parameters, however, are not genuinely linked to reaction mechanisms and are thus hardly useful for any insight into the course of reactions. The degree of cure, i.e., the conversion equivalent, is not referred to the conversion of specific species present in the vulcanization compound, although it is a lumped representation of crosslinks of various lengths formed during the curing of elastomers.

On the other hand, the mechanistic approach has its foundations in the reaction chemistry and mechanisms. The first in-depth study and the most widely recognized reaction scheme was proposed by Coran.[8] The kinetics is represented by accelerator chemistry, crosslinking chemistry, and the scorch-delay. This scheme, though, successfully describes only the over-cure region with equilibrium character. Ding et al.[9] therefore introduced a competitive parallel reaction to crosslink formation, providing explanation for the formation of inactive side products which overall reduce the number of crosslinks directly responsible for rubber network elasticity. Since the reversion was not considered in this last scheme, Ding and Leonov[10] proposed yet another reaction scheme, adding a consecutive reaction to crosslinking. This scheme takes into account the crosslink decomposition reaction that is network degradation. Nevertheless, it still does not consider to explicitly include sulfur and the influence of its amount added to the vulcanization compound on the cure curve. Furthermore, since a lumped representation of the accelerator and its reaction products is used, an accurate relation between accelerator concentration and crosslink density is not established, and also different lengths of polysulfidic chains are not taken into account. Several steps of accelerator chemistry are simply considered nonlimiting and thus negligible in comparison with other reactions, which is not always true. A great step forward was made in a review article by Ghosh et al.[3] An overview of different reactions and their mechanisms has been made for sulfur vulcanization of natural rubber (NR) in benzothiazole accelerated formulations. They developed a model consisting of population balance equations for various species present in the system during vulcanization and estimated the looping probability using a conformational analysis. Great progress has been made by introducing this model as the most comprehensive and detailed one to date, yet as it is stated in the article, the model still assumes the rate of formation or breakage of all the S—S bonds to be independent of the position of the bond from the ends of the molecule, which is not entirely accurate. The reactivity of all polysulfidic molecules of a particular type was assumed to be similar for a particular reaction regardless of the end group. This is true, except in the case of sulfur radicals or other active forms of reactive species which are too close to the end group, so that its effect is not diminished by its remoteness. In this, as well as in previous less-detailed studies of vulcanization kinetics, heat transfer is not incorporated into the model; yet it remains one of the factors responsible for scorch-delay because of the initial thermal equilibration of the vulcanization compound, which is also responsible for the decrease of the storage modulus often used to indirectly track the course of vulcanization and crosslink formation.

Deiber et al.[11,12] proposed a model which would incorporate kinetics as well as heat transfer during the vulcanization. They developed a model for an oscillating bicone cell using adaptable kinetic and heat transfer parameters, resulting in good agreement between the model predictions and experimental results. Nevertheless, the kinetic model applied was represented by the overall macrokinetic expression. This did not only reduce a great number of reactions into a single expression, the reversion was not taken into account as well, considering only the over-cure region with equilibrium character.

The goal of this work was to develop a kinetic model which would take into account the exact location in the molecule where the reaction takes place, to successfully describe the behavior of the storage modulus in regions where heat transfer, kinetics, or both contributions are a decisive factor, to include the reactions of more accelerators into the reaction scheme and finally to study the effect of the polybutadiene rubber (BR)/NR ratio in the initial blend on the crucial reactions in terms of activation energies and constants for specific reactions at various ratios.

EXPERIMENTAL

When studying the vulcanization kinetics and heat transfer the filler was omitted in vulcanization formulation to annihilate its influence on the vulcanization process. The filler modifies the product properties; however, it may also be disputed if the kinetic parameters extracted from the kinetic model would have any meaning considering the nature of their determination through rheological properties, which are undoubtedly strongly dependant on filler and its concentration. All components for vulcanization were stored at low temperature. They were mixed into the rubber on the Brabender Plasti-Corder PLD-Type 651 instrument equipped with the W 50 C measuring mixer with maximum torque 100 Nm at 100°C. The applied mixing temperature was moderately low as we observed that at 140°C there was practically no vulcanization present, whereas at 100°C mixing was performed for only 10 min. Thus the processes occurring during mixing are more of a physical than of a chemical nature, the latter being limited to a rather

small extent. After all model parameters have been calculated, the calculated error occurring due to overlooked chemical processes during mixing was found to be negligible. The formulation of the rubber compounds is presented in Table I.

A very high cis homopolymer BR, with density of 910 kg/m^3 and $\overline{M}_w$ of 6.0 $\times$ 10^5 g/mol and a polyisoprene (NR), with density of 920 kg/m^3 and $\overline{M}_w$ of 8.2 $\times$ 10^5 g/mol were used as rubber compounds. The accelerators used were *N*-*t*-butylbenzothiazole-sulfenamide (TBBS; industrial name Westco TBBS from Western Reserve Chemical) with a density of 1280 kg/m^3 and *N*,*N*-di-*t*-butylbenzothiazole-sulfenamide (TBSI; industrial name Santocure TBSI from Akzo Nobel Chemicals) with a density of 1350 kg/m^3. A mixed *N*,*N*′-diaryl-*p*-phenylenediamine (DTPD; industrial name Vulkanox 3100 from Bayer) with a density of 1200 kg/m^3 and *N*-(cyclohexylthio)phtalimide (CTP; industrial name Westco CTP from Western Reserve Chemical) with a density of 1300 kg/m^3 were used as antioxidant and retarder, respectively.

Vulcanization of prepared samples was performed on the RPA 2000 instrument (Alpha Technologies) and DSC 821^e instrument (Mettler Toledo). During rubber process analyzer (RPA) measurement conditions were isothermal with the exception of initial thermal equilibration. The samples underwent dynamic oscillation at 7% strain amplitude and 0.1 Hz frequency. The temperatures of cure meter plates were set to 160°C, 170°C, and 180°C for all samples and additionally to 140°C, 150°C, and 190°C for pure BR samples. Sample formulations 1–10 (Table I) were measured on RPA with the bicone cell measuring system for 30–60 min, depending on the sample.

Dynamic scanning calorimetry (DSC) measurements were conducted under isothermal conditions in a nitrogen atmosphere. DSC scans were performed at 160°C, 170°C, and 180°C for sample formulations 1–15, and pure unmixed samples of all weight ratios. The samples were put in 40-μL aluminum crucibles with a pin and vulcanized for 30–60 min.

IR spectra of various accelerator and retarder compounds were obtained from the 2000 NR FTIR spectrometer (Perkin–Elmer) using a high temperature measuring cell. The samples were prepared by mixing TBBS, TBSI, or TBBS + CTP with the inert KBr. Sample spectra were then collected over a period of time (30 min) and the spectra evaluated with Spectrum 5.0.1.

HyperChem 7.5 was used for molecular modeling, and Matlab 7.1 was used for numerical computations and modeling.

TABLE I
Formulation of Rubber Compounds

	Compound														
	1	2	3	4	5	6	7	8	9	10	11	12	13	14	15
Ingredients															
BR (butadiene rubber) (g)	100	75	50	25	0	100	75	50	25	0	100	75	50	25	0
NR (natural rubber) (g)	0	25	50	75	100	0	25	50	75	100	0	25	50	75	100
TBBS (accelerator) (g)	2.05	2.05	2.05	2.05	2.05	2.05	2.05	2.05	2.05	2.05	–	–	–	–	–
TBSI (accelerator) (g)	0.82	0.82	0.82	0.82	0.82	0.82	0.82	0.82	0.82	0.82	–	–	–	–	–
CTP (retarder) (g)	0.10	0.10	0.10	0.10	0.10	0.10	0.10	0.10	0.10	0.10	–	–	–	–	–
Sulfur (g)	0.70	0.70	0.70	0.70	0.70	–	–	–	–	–	–	–	–	–	–
ZnO (with fatty acids) (g)	2.36	2.36	2.36	2.36	2.36	2.36	2.36	2.36	2.36	2.36	–	–	–	–	–
ZnO (French procedure) (g)	1.00	1.00	1.00	1.00	1.00	1.00	1.00	1.00	1.00	1.00	–	–	–	–	–
Stearic acid (g)	2.00	2.00	2.00	2.00	2.00	2.00	2.00	2.00	2.00	2.00	–	–	–	–	–
DTPD (anti-oxidant) (g)	1.50	1.50	1.50	1.50	1.50	1.50	1.50	1.50	1.50	1.50	–	–	–	–	–
Cumulative weight (g)	110.53	110.53	110.53	110.53	110.53	109.83	109.83	109.83	109.83	109.83	100.00	100.00	100.00	100.00	100.00

Vulcanization model

Reaction kinetics

The objective of the paper by Ghosh et al.[3] was to initiate the development of a quantitative, fundamental

TABLE II
Reaction Scheme for Sulfur Vulcanization of Polybutadiene and Natural Rubber with Accelerators TBBS and TBSI

Accelerator chemistry	
$TBBS \xrightarrow{k_{TBBS}} MBT + amine$	(R.1)
$TBSI \xrightarrow{k_{TBBS}} MBT + TBBS$	(R.2)
$TBBS + MBT \xrightarrow{k_{TBBS-MBT}} A_0 + amine$	(R.3)
$TBSI + MBT \xrightarrow{k_{TBSI-MBT}} A_0 + TBBS$	(R.4)
$A_X \xrightarrow{k_B} E^*_Y + E^*_Z \quad 0 \le X \le 14 \quad X = Y + Z$	(R.5)
$A_0 + A_X \xleftrightarrow{k_{A-A}} A_Y + A_Z \quad 0 \le X \le 14 \quad X = Y + Z$	(R.6)
Crosslinking chemistry	
$A_X + rubber \xrightarrow{k_{A-R}} B_X + MBT \quad 0 \le X \le 14$	(R.7)
$B_X \xrightarrow{k_{B-R}} B^*_Y + E^*_Z \quad 1 \le X \le 16 \quad X = Y + Z$	(R.8)
$B^*_X + rubber \xrightarrow{k_{VU}} Vu_X \quad 1 \le X \le 16$	(R.9)
Post-crosslinking chemistry	
$Vu_X \xrightarrow{k_{DEG}} deadends \quad 2 \le X \le 16$	(R.10)
$Vu_X + A_0 \xrightarrow{k_{DESULF}} Vu_{X-1} + A_1 \quad 2 \le X \le 16$	(R.11)
Retarder chemistry	
$CTP + MBT \xrightarrow{k_{RET}} CDB + phtalimide$	(R.12)
$CDB + MBT \xrightarrow{k_{CDB}} A_0 + cyclohexylhydrodisulfide$	(R.13)
Other reactions	
$E^*_X + S_Y \xrightarrow{k_{E-S}} E^*_{X+1} + S_{Y-1} \quad 0 \le X \le 15 \quad 1 \le Y \le 8$	(R.14)
$E^*_X + rubber \xrightarrow{k_{E-R}} B_X \quad 0 \le X \le 16$	(R.15)
$B^*_X + S_Y \xrightarrow{k_{BST-S}} B^*_{X+1} + S_{Y-1} \quad 0 \le X \le 15 \quad 1 \le Y \le 8$	(R.16)
$B^*_X \xrightarrow{k_{LOOP}} L_X(deadend_X) \quad 1 \le X \le 16$	(R.17)
$B^*_X + A_0 \xrightarrow{k_{A-BST}} B_X + E^*_0 \quad 1 \le X \le 16$	(R.18)
$E^*_Y + E^*_Z \xrightarrow{k_{E-E}} A_X \quad 0 \le X \le 14 \quad X = Y + Z$	(R.19)

kinetic model for accelerated sulfur vulcanization. The key requirements of this approach included the relevant chemical reaction mechanisms which were applied, explicit incorporation of the polysulfidic nature of the various molecular species, and critical analysis of the structure of the model to ensure that the kinetic model was the most parsimonious description of the single accelerator vulcanization process of NR consistent with the chemical reaction mechanisms.

The kinetic model for a vulcanization system with two accelerators, developed in this work, assumes the reaction of TBBS in one step forming 2-mercaptobenzothiazole (MBT) and amine products with a competitive reaction of TBBS with MBT. TBSI, on the other hand, reacts in two steps; the first one, which yields MBT and TBBS and the second one, which is actually the previously described TBBS chemistry. The first step of TBSI dissociation is accompanied by a parallel reaction of TBSI with MBT, analogous to TBBS. The reaction scheme for NR or BR vulcanization with two accelerators, that is TBBS and TBSI, sulfur, and retarder is presented in Table II. CDB is 2-(cyclohexyldisulfanyl)-1,3-benzothiazole, and amine is actually 2-amino-2-methylpropane. The formation of dead ends can be attributed to a number of reactions such as formation of inactive pendant groups, sulfur loops (L_X, loop with X sulfur atoms), etc. A_X represents accelerator polysulfide or the zinc-accelerator complex, B_X the crosslink precursor, B^*_X the activated form of the crosslink precursor, Vu_X the crosslink, E^*_X the accelerator-terminated polysulfidic radical and S_Y Y-connected sulfur atoms (elemental sulfur in the case when Y is 8). The kinetic constants ascribed to each reaction in Table II apply solely to the reactions where the end-group effect in the molecule or radical species is negligible, that is, if the polysulfidic chain is long enough. Taking this into consideration, each reaction, where indexed species are involved, is kinetically treated individually, as will be discussed later on, and not in a lumped manner as it was the praxis in former works.[3,8–10] The reaction scheme, however, only offers a generalized review of all crucial reactions for individual vulcanization stages or the overall process. Though this is not explicitly presented in the reaction scheme, the rate constants naturally vary with temperature. The temperature effect was incorporated in the model by means of energy balance, hence upgrading previous mechanistic models. Although these models generally allow nonisothermal conditions, i.e., rate constants represented by the Arrhenius equation, the nonisothermal conditions in the induction phase were often regarded as negligible and thus unaccounted for, with the rate constants maintaining the same value throughout the whole vulcanization process.[3,8–10]

According to Reactions 1–19 the corresponding rate equations, and consequently, the component mass bal-

ance equations for various species which are involved in the vulcanization process, for the batch system, may be written as

$$\frac{d[\mathrm{TBBS}]}{dt} = -k_{\mathrm{TBBS}}[\mathrm{TBBS}] - k_{\mathrm{TBBS-MBT}}[\mathrm{MBT}][\mathrm{TBBS}] + k_{\mathrm{TBSI}}[\mathrm{TBSI}] + k_{\mathrm{TBSI-MBT}}[\mathrm{MBT}][\mathrm{TBSI}] \quad (1)$$

$$\frac{d[\mathrm{TBSI}]}{dt} = -k_{\mathrm{TBSI}}[\mathrm{TBSI}] - k_{\mathrm{TBSI-MBT}}[\mathrm{MBT}][\mathrm{TBSI}] \quad (2)$$

$$\frac{d[\mathrm{MBT}]}{dt} = k_{\mathrm{TBBS}}[\mathrm{TBBS}] + k_{\mathrm{TBSI}}[\mathrm{TBSI}] - k_{\mathrm{TBBS-MBT}}[\mathrm{MBT}][\mathrm{TBBS}] - k_{\mathrm{TBSI-MBT}}[\mathrm{MBT}][\mathrm{TBSI}] + k_{\mathrm{A-R},0}[\mathrm{A}_0] + 2\sum_{i=1}^{14} k_{\mathrm{A-R},i}[\mathrm{A}_i] - k_{\mathrm{RET}}[\mathrm{MBT}][\mathrm{CTP}] - k_{\mathrm{CDB}}[\mathrm{MBT}][\mathrm{CDB}] \quad (3)$$

$$\frac{d[\mathrm{A}_0]}{dt} = k_{\mathrm{TBBS-MBT}}[\mathrm{MBT}][\mathrm{TBBS}] + k_{\mathrm{TBSI-MBT}}[\mathrm{MBT}][\mathrm{TBSI}] - [\mathrm{A}_0]\sum_{i=2}^{14}\sum_{j=1}^{i-1} k_{\mathrm{A-A},0,i,0,j}[\mathrm{A_i}] - k_{\mathrm{A-R},0}[\mathrm{A}_0] - [\mathrm{A}_0]\sum_{i=1}^{16} k_{\mathrm{A-BST},i}[\mathrm{B}_i^*] + k_{\mathrm{E-E},0,0}[\mathrm{E}_0^*]^2 - [\mathrm{A}_0]\sum_{i=2}^{16} k_{\mathrm{DESULF},i}[\mathrm{Vu}_i] + \sum_{i=1}^{13}\sum_{j=1}^{14-i} k_{\mathrm{A-A},i,j,0,0} \times [\mathrm{A}_i][\mathrm{A}_j] + k_{\mathrm{CDB}}[\mathrm{MBT}][\mathrm{CDB}] - k_{\mathrm{B},0,0}[\mathrm{A}_0] \quad (4)$$

$$\frac{d[\mathrm{A}_1]}{dt} = -2k_{\mathrm{A-R},1}[\mathrm{A}_1] + 2[\mathrm{A}_0]\sum_{i=2}^{14} k_{\mathrm{A-A},0,i,0,1}[\mathrm{A}_i] + [\mathrm{A}_0]\sum_{i=2}^{16} k_{\mathrm{DESULF},i}[\mathrm{Vu}_i] - 2[\mathrm{A}_1]\sum_{i=1}^{13} k_{\mathrm{A-A},1,i,0,0}[\mathrm{A}_i] + (k_{\mathrm{E-E},0,1} + k_{\mathrm{E-E},1,0})[\mathrm{E}_0^*][\mathrm{E}_1^*] - (k_{\mathrm{B},0,1} + k_{\mathrm{B},1,0})[\mathrm{A}_1] \quad (5)$$

For $2 \le x \le 13$:

$$\frac{d[\mathrm{A}_x]}{dt} = -2k_{\mathrm{A-R},x}[\mathrm{A}_x] + 2[\mathrm{A}_0]\sum_{i=x+1}^{14} k_{\mathrm{A-A},0,i,0,x}[\mathrm{A}_i] - [\mathrm{A}_0][\mathrm{A}_x]\sum_{i=1}^{x-1} k_{\mathrm{A-A},0,x,0,i} - 2[\mathrm{A}_x]\sum_{i=1}^{14-x} k_{\mathrm{A-A},x,i,0,0}[\mathrm{A}_i] + \sum_{i=0}^{x} k_{\mathrm{E-E},i,x-i}[\mathrm{E}_i^*][\mathrm{E}_{x-i}^*] + \sum_{i=1}^{x-1} k_{\mathrm{A-A},i,x-i,0,0}[\mathrm{A}_i][\mathrm{A}_{x-i}] - [\mathrm{A}_x]\sum_{i=0}^{x} k_{\mathrm{B},i,x-i} \quad (6)$$

For $x = 14$:

$$\frac{d[\mathrm{A}_{14}]}{dt} = -2k_{\mathrm{A-R},14}[\mathrm{A}_{14}] - [\mathrm{A}_0][\mathrm{A}_{14}]\sum_{i=1}^{13} k_{\mathrm{A-A},0,14,0,i} + \sum_{i=0}^{14} k_{\mathrm{E-E},i,14-i}[\mathrm{E}_i^*][\mathrm{E}_{14-i}^*] + \sum_{i=1}^{13} k_{\mathrm{A-A},i,14-i,0,0}[\mathrm{A}_i][\mathrm{A}_{14-i}] - [\mathrm{A}_{14}]\sum_{i=0}^{14} k_{\mathrm{B},i,14-i} \quad (7)$$

For $x = 0$:

$$\frac{d[\mathrm{E}_0^*]}{dt} = \sum_{i=1}^{16} k_{\mathrm{B-R},i,0}[\mathrm{B}_i] - k_{\mathrm{E-R},0}[\mathrm{E}_0^*] - [\mathrm{E}_0^*]\sum_{i=0}^{14}(k_{\mathrm{E-E},0,i} + k_{\mathrm{E-E},i,0})[\mathrm{E}_i^*] - [\mathrm{E}_0^*]\sum_{i=1}^{8} k_{\mathrm{E-S},0,i,}[\mathrm{S}_i] + [\mathrm{A}_0]\sum_{i=1}^{16} k_{\mathrm{A-BST},i}[\mathrm{B}_i^*] + \sum_{i=0}^{14}(k_{\mathrm{B},0,i} + k_{\mathrm{B},i,0})[\mathrm{A}_i] \quad (8)$$

For $1 \le x \le 14$:

$$\frac{d[\mathrm{E}_x^*]}{dt} = \sum_{i=x+1}^{16} k_{\mathrm{B-R},i-x,x}[\mathrm{B}_i] - k_{\mathrm{E-R},x}[\mathrm{E}_x^*] - [\mathrm{E}_x^*]\sum_{i=1}^{8} k_{\mathrm{E-S},x,i}[\mathrm{S}_i] + [\mathrm{E}_{x-1}^*]\sum_{i=1}^{8} k_{\mathrm{E-S},x-1,i}[\mathrm{S}_i] - [\mathrm{E}_x^*]\sum_{i=0}^{14-x}(k_{\mathrm{E-E},x,i} + k_{\mathrm{E-E},i,x})[\mathrm{E}_i^*] + \sum_{i=x}^{14}(k_{\mathrm{B},x,i-x} + k_{\mathrm{B},i-x,x})[\mathrm{A}_i] \quad (9)$$

For $x = 15$:

$$\frac{d[\mathrm{E}_{15}^*]}{dt} = k_{\mathrm{B-R},1,15}[\mathrm{B}_{16}] - k_{\mathrm{E-R},15}[\mathrm{E}_{15}^*] - [\mathrm{E}_{15}^*] \times \sum_{i=1}^{8} k_{\mathrm{E-S},15,i}[\mathrm{S}_i] + [\mathrm{E}_{14}^*]\sum_{i=1}^{8} k_{\mathrm{E-S},14,i}[\mathrm{S}_i] \quad (10)$$

For $x = 16$:

$$\frac{d[\mathrm{E}_{16}^*]}{dt} = -k_{\mathrm{E-R},16}[\mathrm{E}_{16}^*] + [\mathrm{E}_{15}^*]\sum_{i=1}^{8} k_{\mathrm{E-S},15,i}[\mathrm{S}_i] \quad (11)$$

For $x = 0$:

$$\frac{d[\mathrm{B}_0]}{dt} = k_{\mathrm{A-R},0}[\mathrm{A}_0] + k_{\mathrm{E-R},0}[\mathrm{E}_0^*] \quad (12)$$

TABLE III
RPA Characteristics, Measurement Conditions, and Rubber Properties

Area between instrument measuring cell and sample, A[13,14]	31.048 cm^2
Sample volume, V[13,14]	3.5 cm^3
Volume of sample subjected to deformation per sample volume, V'/V[11–14]	0.82
Initial sample temperature, T_i	100°C
Set temperature, T_0	140–190°C
Oscillation frequency, ω	0.628 s^{-1}
Strain rate amplitude, $\dot{\gamma}_0$	0.0440 s^{-1}
Strain amplitude, γ_0	0.07
Rubber density, ρ[15]	920 kg/m^3 (NR), 910 kg/m^3 (BR)
Rubber heat capacity, C_V at T_0[15,16]	1905 J/kg K (NR), 647 J/kg K (BR)
α[15,16]	3.54 $J/kg\ K^2$ (NR), 5.13 $J/kg\ K^2$ (BR)

For $1 \leq x \leq 14$:

$$\frac{d[\mathrm{B}_x]}{dt} = 2k_{\mathrm{A-R},x}[\mathrm{A}_x] - [\mathrm{B}_x]\sum_{i=0}^{x-1} k_{\mathrm{B-R},x-i,i} + k_{\mathrm{E-R},x}[\mathrm{E}_x^*] + k_{\mathrm{A-BST},x}[\mathrm{A}_0][\mathrm{B}_x^*] \quad (13)$$

For $x = 15$ and 16:

$$\frac{d[\mathrm{B}_x]}{dt} = -[\mathrm{B}_x]\sum_{i=0}^{x-1} k_{\mathrm{B-R},x-i,i} + k_{\mathrm{E-R},x}[\mathrm{E}_x^*] + k_{\mathrm{A-BST},x}[\mathrm{A}_0][\mathrm{B}_x^*] \quad (14)$$

For $x = 1$:

$$\frac{d[\mathrm{B}_1^*]}{dt} = \sum_{i=1}^{16} k_{\mathrm{B-R},1,i-1}[\mathrm{B}_i] - (k_{\mathrm{VU},1} + k_{\mathrm{LOOP},1})[\mathrm{B}_1^*] - [\mathrm{B}_1^*]\sum_{i=1}^{8} k_{\mathrm{BST-S},1,i}[\mathrm{S}_i] - k_{\mathrm{A-BST},1}[\mathrm{A}_0][\mathrm{B}_1^*] \quad (15)$$

For $2 \leq x \leq 15$:

$$\frac{d[\mathrm{B}_x^*]}{dt} = \sum_{i=x}^{16} k_{\mathrm{B-R},x,i-x}[\mathrm{B}_i] - (k_{\mathrm{VU},x} + k_{\mathrm{LOOP},x})[\mathrm{B}_x^*] - [\mathrm{B}_x^*]\sum_{i=1}^{8} k_{\mathrm{BST-S},x,i}[\mathrm{S}_i] + [\mathrm{B}_{x-1}^*] \times \sum_{i=1}^{8} k_{\mathrm{BST-S},x-1,i}[\mathrm{S}_i] - K_{\mathrm{A-BST},x}[\mathrm{A}_0][\mathrm{B}_x^*] \quad (16)$$

For $x = 16$:

$$\frac{d[\mathrm{B}_{16}^*]}{dt} = k_{\mathrm{B-R},16,0}[\mathrm{B}_{16}] - (k_{\mathrm{VU},16} + k_{\mathrm{LOOP},16})[\mathrm{B}_{16}^*] + [\mathrm{B}_{15}^*] \times \sum_{i=1}^{8} k_{\mathrm{BST-S},15,i}[\mathrm{S}_i] - k_{\mathrm{A-BST},16}[\mathrm{A}_0][\mathrm{B}_{16}^*] \quad (17)$$

For $x = 1$:

$$\frac{d[\mathrm{Vu}_1]}{dt} = k_{\mathrm{VU},1}[\mathrm{B}_1^*] + k_{\mathrm{DESULF},2}[\mathrm{A}_0][\mathrm{Vu}_2] \quad (18)$$

For $2 \leq x \leq 15$:

$$\frac{d[\mathrm{Vu}_x]}{dt} = k_{\mathrm{VU},x}[\mathrm{B}_x^*] - k_{\mathrm{DEG},x}[\mathrm{Vu}_x] - k_{\mathrm{DESULF},x}[\mathrm{A}_0][\mathrm{Vu}_x] + k_{\mathrm{DESULF},x+1}[\mathrm{A}_0][\mathrm{Vu}_{x+1}] \quad (19)$$

For $x = 16$:

$$\frac{d[\mathrm{Vu}_{16}]}{dt} = k_{\mathrm{VU},16}[\mathrm{B}_{16}^*] - k_{\mathrm{DEG},16}[\mathrm{Vu}_{16}] - k_{\mathrm{DESULF},16}[\mathrm{A}_0][\mathrm{Vu}_{16}] \quad (20)$$

$$d[\text{dead ends}] = \sum_{i=2}^{16} k_{\mathrm{DEG},i}[\mathrm{Vu}_i] + \sum_{i=1}^{16} k_{\mathrm{LOOP},i}[\mathrm{B}_i^*] \quad (21)$$

For $1 \leq x \leq 7$:

$$\frac{d[\mathrm{S}_x]}{dt} = -[\mathrm{S}_x]\sum_{i=0}^{15} k_{\mathrm{E-S},i,x}[\mathrm{E}_i^*] + [\mathrm{S}_{x+1}]\sum_{i=0}^{15} k_{\mathrm{E-S},i,x+1}[\mathrm{E}_i^*] - [\mathrm{S}_x]\sum_{i=1}^{15} k_{\mathrm{BST-S},i,x}[\mathrm{E}_i^*] + [\mathrm{S}_{x+1}]\sum_{i=1}^{15} k_{\mathrm{BST-S},i,x+1}[\mathrm{E}_i^*] \quad (22)$$

For $x = 8$:

$$\frac{d[S_8]}{dt} = -[\mathrm{S}_8]\sum_{i=0}^{15} k_{\mathrm{E-S},i,8}[E_i^*] - [\mathrm{S}_8]\sum_{i=1}^{15} k_{\mathrm{BST-S},i,8}[E_i^*] \quad (23)$$

$$\frac{d[\mathrm{CTP}]}{dt} = -k_{\mathrm{RET}}[\mathrm{MBT}][\mathrm{CTP}] \quad (24)$$

$$\frac{d[\mathrm{CDB}]}{dt} = k_{\mathrm{RET}}[\mathrm{MBT}][\mathrm{CTP}] - k_{\mathrm{CDB}}[\mathrm{MBT}][\mathrm{CDB}] \quad (25)$$

$$\frac{d[\mathrm{amine}]}{dt} = k_{\mathrm{TBBS}}[\mathrm{TBBS}] + k_{\mathrm{TBBS-MBT}}[\mathrm{TBBS}][\mathrm{MBT}] \quad (26)$$

$$\frac{d[\mathrm{phtalimide}]}{dt} = k_{\mathrm{RET}}[\mathrm{CTP}][\mathrm{MBT}] \quad (27)$$

$$\frac{d[\mathrm{cyclohexylhydrodisulfide}]}{dt} = k_{\mathrm{CDB}}[\mathrm{CDB}][\mathrm{MBT}] \quad (28)$$

with initial conditions [TBBS] = [$TBBS_0$], [TBSI] = [$TBSI_0$], [S_8] = [$S_{8,0}$], and [CTP] = [CTP_0], whereas the concentration of all other species is zero in the initial rubber compound.

Energy balance

The temperature of the vulcanization compound changes due to exothermal and endothermal reactions which yields various reaction intermediates and precursors as well as the main and unwanted reaction products. Overall, heat is generated during vulcanization, which is clearly seen on DSC thermograms as an exothermal peak. During vulcanization on the moving die rheometer (MDR) or the oscillating disc rheometer (ODR), heat is also generated because of friction between the cones and the sample surface, as well as due to mechanical energy dissipation inside the sample. The friction term is of course omitted if vulcanization in an industrial vulcanization mold is considered, since there are no moving elements to cause friction in conventional molds. To extract the relevant parameters, which may be used for the scale-up of the vulcanization process, friction energy dissipation has to be considered as an essential part of energy balance, though it is small in contribution. Besides this, one must also consider heat flow from the mold or rheometer wall onto the rubber matrix at an early stage of reaction and heat removal during the curing reactions. When this is put into an energy balance, one obtains

$$\frac{d(\rho V C_v T)}{dt} = h(X(t))A(T_0 - T) + \rho V \Delta H_{\text{tot}} \frac{dX(t)}{dt} + \dot{W} \tag{29}$$

which after rearranging yields the set of differential equations representing the energy balance

$$\frac{dT}{dt} = \frac{h_0(1 + K_1 X(t))A(T_0 - T) + \rho V \Delta H_{\text{tot}}(dX(t)/dt) + V'\dot{\gamma}_0^2(\eta' \cos^2(\omega t) + \eta'' \sin(\omega t)\cos(\omega t))}{\rho V(C_v + T\alpha)} \tag{30}$$

$$\frac{dC_v}{dT} = \alpha \tag{31}$$

with the corresponding initial conditions $T(t = 0) = T_i$ and $C_v(t = 0) = C_v(T = T_i)$.

In eqs. (29)–(31), $X(t)$ represents degree of cure, T represents average sample temperature, and h and h_0 represent average heat transfer coefficients at $X(t)$ and $X(t) = 0$, respectively. ΔH_{tot} is the measured overall heat generated due to chemical reactions, $\dot{W}$ represents energy dissipation within the sample, and η' and η'' are dynamic and out-of-phase viscosity, respectively. K_1 is an adjustable parameter determining how average heat transfer coefficient varies with $X(t)$. Other parameters occurring eqs. (29)–(31) are presented in Table III.

The premise of energy balance is that there is no temperature profile within the sample, that is, the temperature within the sample is basically uniform which is of course not entirely true. However, if the sample thickness versus heat transfer area between the instrument and the sample are considered, the simplification of spatially invariant temperature may be justified.

RESULTS AND DISCUSSION

Since a distinction had to be made between reaction rates of chemically similar species, which generally react according to the same reaction mechanism (for example reaction of A_0 or A_1 with rubber, consistent with R. 7), molecular modeling was applied. Our goal was to find stable conformations that are optimized geometries for a variety of species that are produced during vulcanization or directly added to the rubber compound only to react with rubber itself and among themselves according to the reaction scheme. This was achieved by semiempirical PM3 method calculations, using unrestricted Hartree–Fock spin pairing and self-consistent field controls of 0.001 convergence limit and 1000 iterations limit. Furthermore, the Polak–Ribiere (conjugate gradient) algorithm was applied. Generalized geometries of all species subjected to geometry optimization are presented in Figures 1(a)–1(e). Instead of rubber chains with an infinite number of repeating monomer units, a sequence of five units of isoprene or butadiene was used as the rubber component model. This is a sufficiently long chain, since our calculations with longer chains yielded basically no difference in the calculated parameters, such as reaction enthalpy, calculated from heats of formation of all species which reacted or were produced.

After the molecular geometry of all reacting species was successfully optimized, the search for transition state geometry was carried out. Like most other authors, we did not make any distinction between the transition structure (being the geometry at the point of potential energy maximum on the reaction pathway) and the transition state (being the geometry at the maximum of the free energy profile).[8,17–20] This approximation was made on the basis of the calculated activation energies, which were only used as an aid to include the distinction between various similar reacting species into the model. Thus the activation energies were not calculated *per se* and considered as true intrinsic properties of the system, but more with regard to their relative tendency to react depending on the length of the polysulfidic chain. Semiempirical calculations were applied with the same method, as when optimizing geometry of reacting species. Quadratic synchronous

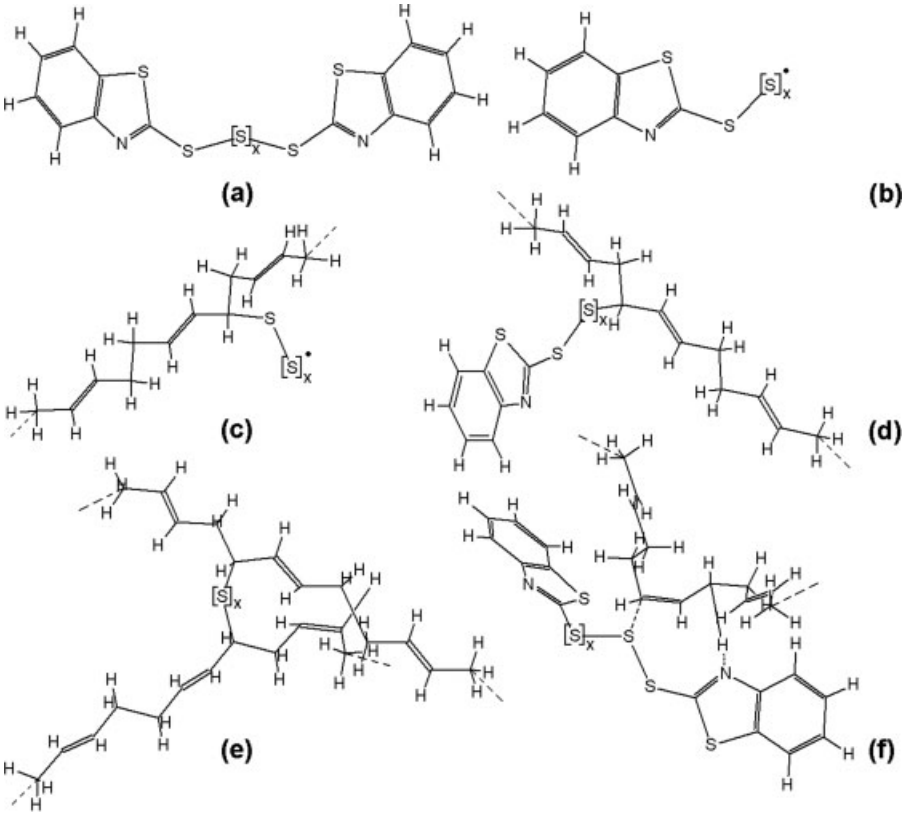

Figure 1 A_X molecule (a), E^*_X molecule (b), B^*_X molecule (c), B_X molecule (d), Vu_X molecule (e), and transition state with an eight-membered ring for R. 7 (f).

transit algorithm was applied. Activation energies were calculated according to Eyring equation, the theoretical construct based on the transition state model, thus

$$E_A = \Delta H^{\#} + RT \tag{32}$$

where $\Delta H^{\#}$ represents the difference between the formation enthalpies of the transition structure and the energy minimum before energy rise towards the transition structure location on the reaction pathway. Preexponential factor (A) is, according to Eyring equation, linked to $\Delta S^{\#}$. However, for our calculations we considered the entropy term negligible and the temperature dependence of A dwarfed by the activation energy term.

Figure 2 represents the variation of activation energy with the locus of the bond scission reaction. As the model is arbitrary, limited to a maximum of 16 sulfur atoms in a polysulfidic chain, the A_X molecule with the greatest number of sulfur atoms is A_{14}. We see that the S—S bonds closest to the benzothiazole group are likely to react slower than the ones further away from this end group. This is probably due to the stability of this bond because of the vicinity of the benzothiazole group which stabilizes the bond through resonance, whereas sulfur atoms in the main chain farther from the end group are not additionally stabilized. However, according to Fairbrother et al.[21] the products of these bonds' scission reactions are stabilized. Activation energy for the cleavage of S—S bonds decreases as the distance from end group increases, yet after a few bonds the decrease of the activation energy levels asymptotically. The maximum number of

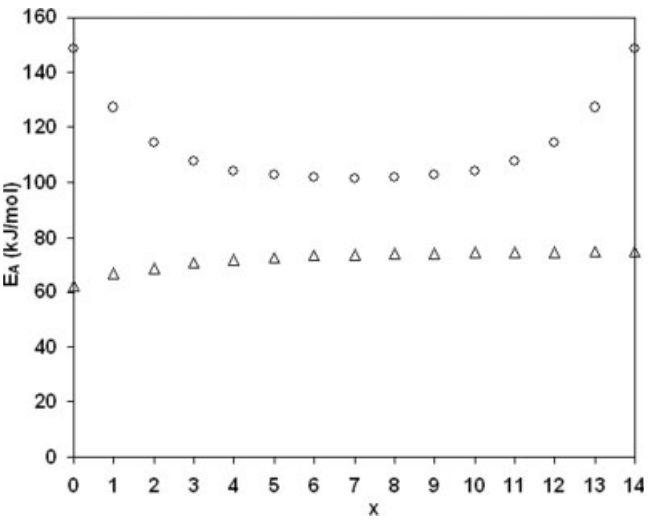

Figure 2 Variation of activation energy of S—S bond cleavage in A_{14} molecule (○) and activation energies for R. 7 as a function of x value in A_X (△).

sulfur atoms in the polysulfidic chain was arbitrarily set to 16. Nevertheless, the molecular modeling results show that the maximum length of polysulfidic chain is sufficient, so that calculated parameters become invariant to end groups as the distance between end group and sulfur bond increases. The symmetry seen on Figure 2 is related to the structure of the A_X molecule presented in Figure 1(a). Modeling of R. 8 was handled virtually in the same manner and the results were analogous to those of R. 5, i.e., gradual lowering of activation energies is observed as the main sulfur backbone is approached, contrary to Coran[8,17] and confirming the recent quantum chemical calculations mentioned by Ghosh et al.[3]

The result of the molecular modeling of R. 6 is a four-dimensional matrix containing activation energies, where two dimensions represent the first and the second reacting molecule and the other two dimensions the location of the bond scission. Some elements of this matrix are not relevant since through the forward R. 6 A_{14} is the longest molecule to react with A_0, having 15 locations of possible bond scission, whereas there is only one possible bond scission of molecule A_0. The forward reaction between A_0 and A_0 or A_0 and A_1 does not take place, since recombination would result in the same species which react, so there is no chemical potential as the driving force when reactants and products are the same molecules, with the same geometry.

During modeling, it was presumed that R. 7 proceeds via nonradical mechanism proposed by Coran,[19,20] where the transition state is an eight-membered ring intermediate, shown in Figure 1(f). The geometry of these transition states was optimized and the activation energies, which were calculated, are presented in Figure 2. Smaller A_X molecules react faster than the ones with a longer polysulfidic chain owing to easier feasibility of ring formation when steric hindrance is less significant, as in the case of the A_0 molecule. When A_X molecules are larger and in the state of the most favorable conformation, probability of ring formation and thus the ring formation reaction rate are diminished.

R. 9 was treated in the same way as R. 7 by looking for a transition state and activation energy calculation when moving along the reaction coordinate, B^*_X attacking the allyl carbon atom in rubber and hydrogen distancing itself from this very same atom. The geometry of the transition state was optimized and the activation energy calculated. Activation energy values progressively become smaller as we increase the distance from end groups. R. 10, R. 11, and R. 14–19 were treated in the same manner, choosing different approaches only to eventually calculate the activation energies and consequently the correction factors, which were used as corrections of kinetic constants in the model, as follows.

It was assumed that all kinetic constants follow the temperature dependency according to Arrhenius law

$$k_{i,j} = \mathrm{cf}_{i,j} A \exp\left(-\frac{E_A}{RT}\right) = \mathrm{cf}_{i,j} k \tag{33}$$

where $k_{i,j}$ is the kinetic constant and $\mathrm{cf}_{i,j}$ the correction factor for the reaction where i and j indexed species are consumed or produced. A, E_A, and k are the pre-exponential factor, the activation energy, and the kinetic constant for the reaction, respectively, where influences of end groups are minimized. To illustrate this principle, reaction $A_{14} \xrightarrow{k_B} E_0^* + E_{14}^*$ may be taken as an example. Apparently an S—S bond in the A_{14} molecule is broken very close to the benzothiazole end group, resulting in different activation energy for the formation of products due to various effects of the end group. The further from the end group along the polysulfidic chain the S—S bond is located, the lesser are the effects of the benzothiazole end group; annihilating the end group influences when the polysulfidic chain is infinitely long or tendencies of asymptotic behavior of reaction activation energies are observed.

Activation energies from molecular modeling calculations were used to define correction factors as

$$\mathrm{cf}_{i,j} = \exp\frac{E_A - E_{A,i,j}}{RT} \tag{34}$$

For the mentioned reaction, $E_{A,i,j}$ would be $E_{A,0,14}$ and E_A the value of activation energy where all values of activation energies converge with elongation of the polysulfidic chain, $E_{A,7,7}$ being the closest value should we limit ourselves to a maximum of 16 sulfur atoms in the polysulfidic chain.

The only exception is R. 6, where the kinetic constant is denoted as $k_{\mathrm{A\text{-}A},i,j,k,l}$ indexes i and j, representing the reacting species A_i and A_j while the other two, k and l, represent the bond of cleavage, 0 being the number of the S—S bond closest to the benzothiazole group. In the same way we defined $\mathrm{cf}_{\mathrm{A\text{-}A},i,j,k,l}$ and $E_{A,\mathrm{A\text{-}A},I,j,k,l}$.

Since there were two accelerators present in the formulations prepared for curing, separate experiments had to be performed to determine the kinetics of accelerator chemistry. For the purpose of studying individual accelerator chemistry kinetics by means of Fourier transform infrared (FTIR) spectroscopy, we prepared a formulation consisting of only one of the accelerators and KBr powder in the same weight ratios as when preparing vulcanization formulations. However, in this case the inert component KBr replaced rubber. KBr thus enabled preparation of samples and made it possible for the concentration of accelerator in the samples to be comparable with that in the vulcanization formulation. In view of the fact that all other components needed for the vulcanization of rubber were

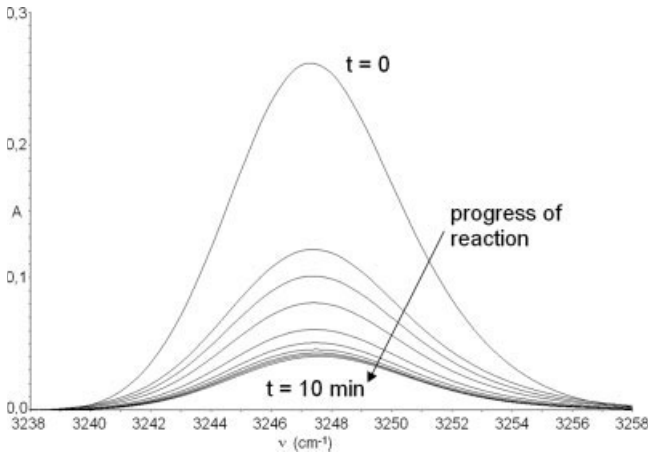

Figure 3 Peak representing the secondary amine group: absorbance at a characteristic wave number lowers with time due to conversion of the secondary amine group into the primary amine group.

not added to the sample, only R. 1, R. 3 and R. 5 (for $x = 0$), or R. 1–4 and R. 5 (for $x = 0$) take place for TBBS and TBSI formulations, respectively. The kinetic model is consequently reduced to eqs. (1), (3), and (4) or eqs. (1)–(4) for TBBS and TBSI, respectively.

According to IR spectroscopy literature,[22] characteristic peaks for functional groups of interest are visible at different wave numbers between 400 and 4000 cm^{-1}. Signal for *t*-butyl group in the TBBS is found at wave numbers 1365 and 1389 cm^{-1} while the amine group characteristic signal may be seen at 3248 cm^{-1}. Besides these signals there are also others, such as the secondary amine group N—H wag, aromatic ring C—H stretches and bends, etc. After reviewing all spectra for TBBS and TBSI at various times and temperatures, however, the two mentioned signals proved to be the most reliable in terms of overlapping with neighboring peaks. The peak at 3248 cm^{-1}, representing a secondary amine group of TBBS, varied with time, while the *t*-butyl peaks remained the same throughout our experiment. No peaks can be observed in the vicinity of 3248 cm^{-1} in the TBSI spectrum, since there is no secondary amine group in the accelerator molecule. FTIR spectra were analyzed at different temperatures and reaction times, especially at characteristic wave numbers, and the results were changing peak heights as shown in Figure 3. Conversions were then calculated from spectra using the Beer–Lambert equation and kinetic constants were calculated at different temperatures. While characteristic peaks of reacting species and products became lower or higher (for example, peak at 3248 cm^{-1} was decreasing with time for the sample, consisting of TBBS, whereas for the TBSI sample it initially rose with time and after a while started to decrease, which corresponds to the initial TBBS formation and consequential depletion of latter), some of the characteristic peaks, representing functional groups, which were not involved in reaction chemistry (*t*-butyl, benzene, etc.), remained the same, thus setting a reference for calculating conversions from FTIR spectra.

The kinetic constants were first calculated for the sample consisting of solely TBBS and the inert component (k_{TBBS} and $k_{TBBS\text{-}MBT}$). These constants were then applied in an extended model for TBSI, calculating another pair of kinetic constants (k_{TBSI} and $k_{TBSI\text{-}MBT}$) analogically to the previously calculated k_{TBBS} and $k_{TBBS\text{-}MBT}$. The amount of TBBS formed from TBSI is most obviously obtained if the behavior of the peak at 3248 cm^{-1} is traced. Moreover if the initial spectrum of TBBS is compared with the one after a relatively long time of reaction at 160°C, it may be observed that the peak in question almost diminishes, providing us a reference concerning the amount of TBBS formed from TBSI according to R. 2, which has not yet reacted further with MBT or simply dissociated. The results are shown in Table IV.

It is evident From Table IV that TBBS and TBSI react practically with the same reaction rate, TBSI being useful for vulcanization because of its bifunctionality resulting in initial formation of MBT and TBBS. The TBBS formed during this reaction reacts even in later stages of the scorch-delay when the TBBS added to the initial vulcanization mixture is gradually depleted. Table IV also shows that the reaction between either primary or secondary accelerator and MBT is a little faster than reaction of accelerator dissociation, making the latter reaction a rate-limiting step of the induction period.

Since the retarder chemistry does not involve any interaction with rubber, that is, both CTP and CDB react with MBT, retarder chemistry kinetics were also studied. Therefore, a sample containing TBBS, from which the reacting MBT is produced, CTP, and an inert component in a suitable weight ratio was prepared. As the characteristic peaks of phtalimide, formed through R. 12, at 3205 cm^{-1} for N—H stretch and 1774 and 1745 cm^{-1} for C=O stretches, overlap with those of

TABLE IV
Kinetic Parameters of Accelerator Chemistry Kinetics

Reaction	TBBS dissociation	TBSI dissociation	Reaction between TBBS and MBT	Reaction between TBSI and MBT
A (s^{-1}) or (L mol^{-1} s^{-1})	0.269	0.243	6.61×10^{11}	8.25×10^{11}
E_A (kJ/mol)	15.5	15.1	87.5	88.3

TABLE V
Kinetic Parameters of Retarder Chemistry Kinetics

Reaction	CTP–MBT reaction	CDB–MBT reaction
A (10^{11}) (L mol^{-1} s^{-1})	1.17	8.25
E_A (kJ/mol)	88.0	88.3

TBBS, the reactions of the retarder could not be dealt with directly. Anyhow, if the model consisting of eqs. (1), (3), (4), and (24)–(28) is considered, where the corresponding suitable reactions are R. 1, R. 3, R. 5 ($x = 0$), R. 12, and R. 13, the FTIR data may be fitted indirectly, since application of the retarder causes partial consumption of generated MBT through R. 12 and R. 13, thus reducing the overall TBBS disappearance rate. The kinetic constants were calculated for the sample consisting of TBBS, CTP, and the inert component (k_{RET} and k_{CDB}). The results are presented in Table V.

If vulcanization of the sample is performed in an oscillating bicone cell and the results critically evaluated, especially the storage modulus, G', one observes that there is an initial drop of G', mostly due to thermal equilibration of the sample, which was concluded from the fact that the locus of G' curve minima (when executing sulfur or sulfur-free vulcanization) is reached at virtually the same times as the derivative of average temperature of the sample reaches zero. It is also visible that the minima of the sulfur and sulfur-free vulcanization process are reached after the same time lapse, making it apparent that the initial G' drop during the induction time should be ascribed mostly to the temperature dependence of mechanical properties of the sample. Since both thermal equilibration and vulcanization process initiation are noninstantaneous, the kinetic model which incorporates the complex kinetics of vulcanization with both accelerators and at the same time does not diminish the role of the average sample temperature and its impact on mechanical properties was developed.

Dependence of rheological quantities on temperature and degree of cure may be described by the following equations:[11,12]

$$G'(t) = G'(T_0)\left(\frac{T}{T_0}\right)^{X(t)} \exp\left(\frac{\Delta H'}{R}\,\frac{T_0 - T}{T_0 T}(1 - X(t))\right) + X(t)(G'(t_{max}) - G'(t_{min})) \quad (35)$$

$$\eta'(t) = \eta'(T_0)\exp\left(\frac{\Delta H''}{R}\frac{T_0 - T}{T_0 T}(1 - X(t))\right) \times \exp(C_1 X(t) + C_2 X(t)^2) \quad (36)$$

$$\eta''(t) = \frac{G'(t)}{\omega} \quad (37)$$

with initial G', η', and η'' defined as $G' = G'(T_i)$, $\eta' = \eta'(T_i)$, and $\eta'' = \frac{G'(T_i)}{\omega}$, where $\Delta H'$, $\Delta H''$, C_1, and C_2 are adjustable model parameters which influence the temperature dependence rheological quantities, and R is the gas constant. Equations (35)–(37) with corresponding initial conditions do not treat rheological quantities from a viewpoint of nonisothermal viscoelasticity but tries to encompass the effect of temperature on these quantities in a manner of general model which sufficiently describes their behavior during induction period.[11,12] During curing period, nevertheless, the conditions are practically isothermal and thus kinetic fitting may be carried out in a rigorous manner. If one now wants to consider both the contribution of the initial ascending temperature of the sample and chemical crosslinking at the same time, it has to be presumed, as was mentioned before, that the reactions present in the course of vulcanization are relatively slow during the initial equilibration period, especially the formation of crosslinks, which is actually a consecutive reaction and directly affects the degree of cure, $X(t)$. This assumption is valid, as the sample reaches its desired end temperature fairly fast and thus $X(t)$ prior to $G'(t)$ minimum being reached is practically zero. In eq. (35) $G'(t)$ is written as a sum of two contributions. Evidently, during the induction period the first term plays the decisive role in determining $G'(t)$ since $X(t)$ is relatively small or practically zero. By using eq. (35), we thus describe the whole vulcanization curve, consisting of the induction, curing, and over-cure period. However, when the sample reaches the temperature of the plates, T_0, the whole expression is reduced to frequently used relation between the degree of cure, $X(t)$, and the storage modulus, where $G'(T_0) = G'(t_{min})$.

$$X(t) = \frac{G'(t) - G'(t_{min})}{G'(t_{max}) - G'(t_{min})} \quad (38)$$

t_{min} and t_{max} are times when the minimum and the maximum of the vulcanization curve are reached, respectively. It is important to clarify the distinction between the degree of cure in macrokinetic models and the one used in mechanistic models. In the first case, $X(t)$ represents overall conversion only and may not be directly linked to chemical reactions, whereas in second case it is a direct measure of relative crosslink concentration, which increases during vulcanization and may be described using one of proposed reaction mechanisms.

Now the relationship between the degree of cure and the concentration of crosslinks per unit of volume only has to be defined as

$$X(t) = \frac{\sum_{x=1}^{16}[\mathrm{Vu}_x]}{\left(\sum_{x=1}^{16}[\mathrm{Vu}_x]\right)_{max}} \quad (39)$$

Since according to the statistical theory of rubber elasticity,[23] the storage modulus, G', which represents elastic contribution opposite to viscous contribution, represented by the loss modulus, G'', is proportional to the average number of network chains contained in a unit of volume.

The model therefore combines the two aspects of vulcanization process. One is heat transfer, which plays a decisive role during the induction period. It is embodied in eqs. (29)–(31) and is related to kinetics through terms including $X(t)$, directly depending on the concentration of crosslinks [eq. (39)], though in the first stage of vulcanization the kinetics of crosslink formation are not as distinctive as in later stages. The second aspect is that kinetics of various reactions are embodied in the component mass balances represented by eqs. (1)–(28) and are related to energy balances as stated. Storage moduli (G'), η', and η'' depend on temperature as well as on the degree of cure according to eqs. (35)–(37), G' being of the greatest importance as it is directly linked to kinetics and heat transfer, since the cure curve is commonly presented by G' versus time.

Developed kinetic model was fitted to experimental data to find the values of model parameters that best agreed with experimental results, where rubber properties and instrument characteristics were obtained from the literature (Table III).

Before and after vulcanization a frequency sweep measurement was made to ensure linear viscoelastic regime. ΔH_{tot} was measured using isothermal DSC technique at temperatures corresponding to that of RPA experiments. These results, however, were of little importance, since practically no heat evolves during the induction period, where energy balance is of great importance. Later on during the cure and over-cure period, vulcanization compound temperature virtually remains the same, that is at set temperature, since the evolved heat is removed from the sample granting isothermal conditions. $G'(T_0)$ and $\eta'(T_0)$ were evaluated for each experiment from RPA experimental data. Figure 4 confirms the validity of the presumption $G'(T_0) = G'(t_{min})$ used to derive eq. (36), as it may be seen that the storage moduli of the BR vulcanization compound with and without added sulfur basically coincide with each other because the initial modulus decrease can be ascribed almost completely to temperature dependence of G', also included in eq. (35). This was confirmed for all BR/NR weight ratios. Later on, as it may be observed, both curves start to separate, since sulfur crosslinks are produced far more intensively in the compound containing sulfur than in the one without it. Moreover, Figure 5 shows measured temperatures of the upper RPA cone (the lower cone temperature is virtually the same), which quite quickly reaches the set temperature, whereas the model predicted that temperature of the sample rises asymptotically towards the set temperature and slightly over it due to exothermal reactions and friction energy dissipation. The temperature of the compound, nevertheless, reaches its set point at the storage modulus minimum, and thus eq. (35) is reduced to eq. (38), which successfully describes the storage modulus behavior only during the cure and the over-cure region, leaving the induction period unaccounted for, whereas eq. (35) encompasses the whole cure curve. $G'(t_{max})$ was also determined from the cure curve. It has to be stressed that the RPA upper cone temperature merely sets a trend towards which sample temperature rises and may not be considered as the sample temperature.

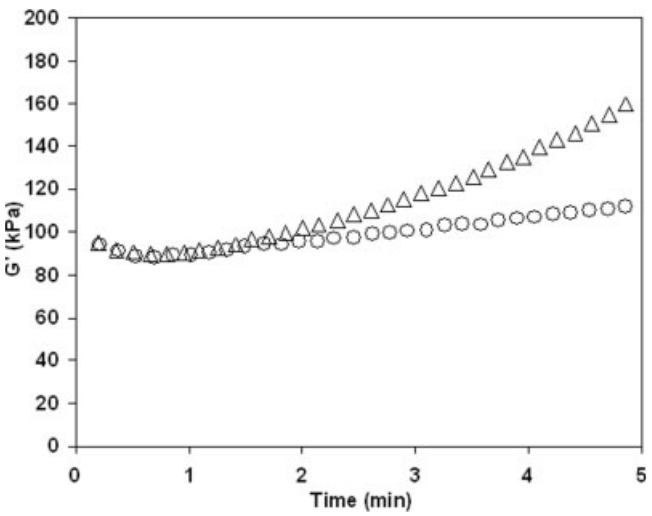

Figure 4 Storage modulus as a function of time for BR vulcanization at 170°C: (△) vulcanization of BR with sulfur; and (○) vulcanization of BR without sulfur.

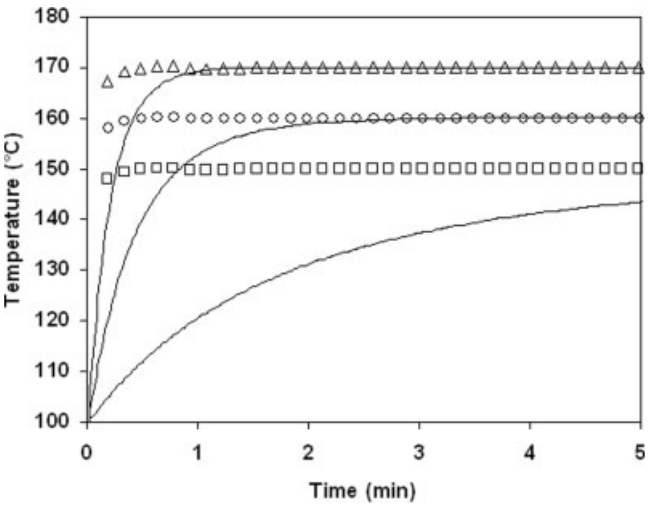

Figure 5 Experimental data for RPA upper cone temperatures and model predictions for BR vulcanization compound temperatures during vulcanization induction: temperature of RPA upper cone at set temperatures 170°C (△); 160°C (○); 150°C (□); and model prediction of vulcanization compound temperature (–).

After assembling all rubber material properties, method parameters, and instrument characteristics, the model was fitted on experimental data. During the induction period, at which the storage modulus changed mostly due to the temperature rise from the initial to the set temperature, G', η', and η'', predicted by the model, were fitted on experimental data, taking into account eqs. (30), (31), (35)–(37). K_1, C_1, and C_2, the arbitrary parameters, may be omitted when the fitting procedure is performed in the initial stage of vulcanization, as $X(t)$ is practically zero. The fitting is thus reduced to only three parameters, h_0, $\Delta H'$, and $\Delta H''$. Levenberg–Marquardt algorithm was applied for optimizing the heat transfer parameters. Since $\Delta H'$ and $\Delta H''$ represent activation energy equivalents in the exponential term of Arrhenius relation, one may justly presume that they should not vary greatly with temperature, which was confirmed when these two parameters were calculated, $\Delta H'$ showing a steady but minute rise when the temperature of vulcanization is elevated from 140°C to 160°C and then somewhat asymptotic behavior oscillating slightly around the value reached at 160°C. The behavior of $\Delta H''$ is similar, suggesting that even though the effect of temperature on $\Delta H'$ and $\Delta H''$ is negligible, there is an initial rise which levels up at 160°C. On the other hand, the BR/NR weight ratio influences these two parameters to some extent so that there is a local minimum and maximum at composition 50 wt % BR–50 wt % NR for $\Delta H'$ and $\Delta H''$, respectively. There is some parallel between this finding and the behavior of h_0 with temperature and composition of the vulcanization compound, as shown in Figure 6. The heat transfer coefficient, h_0, obviously rises from its value between 100 and 150 W/(m^2 K) for pure BR to its value between 250 and 400 W/(m^2 K) for pure NR, the local minimum being at the weight ratio of 50 : 50, where the minimum is the more distinctive the lower the temperature is. This is probably due to the specific interaction between BR and NR phases in the compound at this composition. The rise of h_0 is the greater the higher the applied temperature of vulcanization.

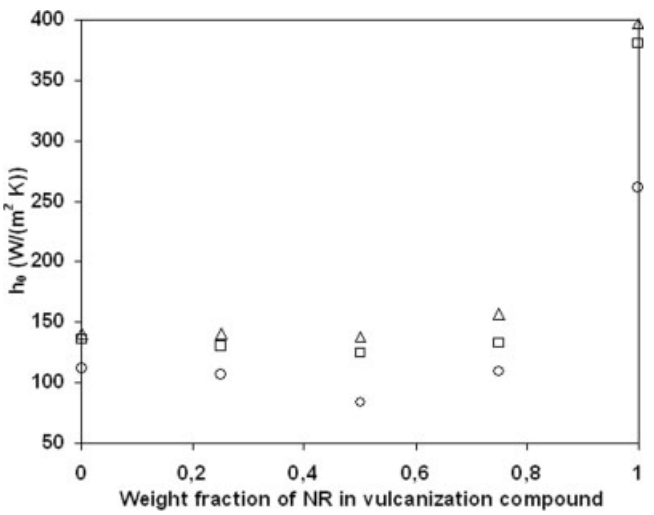

Figure 6 Influence of weight fraction of natural rubber in the vulcanization compound on the heat transfer coefficient: (○) 160°C; (□) 170°C; and (△) 180°C.

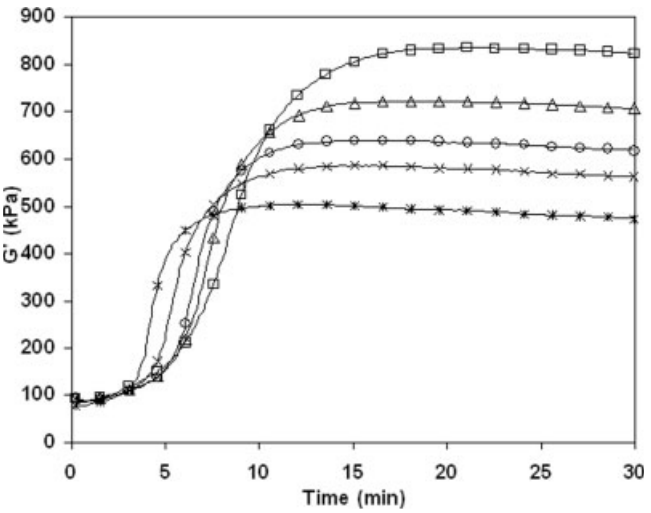

Figure 7 Influence of the vulcanization compound on vulcanization curves at 170°C: (–) vulcanization model; (□) 100% BR; (△) 75% BR/25% NR; (○) 50% BR/50% NR; (×) 25% BR/75% NR; and (*) 100% NR.

After these parameters had been fitted and the induction period behavior of G' sufficiently described, the kinetic constants k_B, $k_{A\text{-}A}$, $k_{A\text{-}R}$, $k_{B\text{-}R}$, k_{Vu}, k_{DEG}, $k_{E\text{-}S}$, and $k_{E\text{-}E}$ were fitted on G' experimental data via eqs. (38) and (39). The degree of cure at G' minimum was set at zero. Further assumptions were $k_{DESULF} = k_{A\text{-}BST} = k_{A\text{-}A}$, $k_{E\text{-}R} = k_{Vu}$, $k_{BST\text{-}S} = k_{E\text{-}S}$, and $k_{LOOP,i} = cf_{R.17,i}\, k_{Vu,i}$. These assumptions are quite justified, since with the introduction of correction factors, these constants are not the same for all lengths of the sulfur backbone in various species, but only for the main chain where the effects of end groups are not present anymore and thus the chemistry of similar reactions is similar and the kinetics comparable, but only if the distance from end groups, either rubber or benzothiazole, is great enough, so that their effect on reaction rates no longer needs to be taken into account. Levenberg–Marquardt algorithm was applied for optimizing the kinetic parameters.

The developed kinetic model describes relatively well the time dependence of the storage modulus during the course of vulcanization. It may be observed in Figure 7 that even for various vulcanization formulations the model well describes the course of rubber mixture curing via agreement between the predicted and the measured values of the storage modulus. On the other hand, we were also interested in the formation of crosslinks over time, as predicted by the model. As reported by Ghosh et al.[3] monosulfidic crosslinks

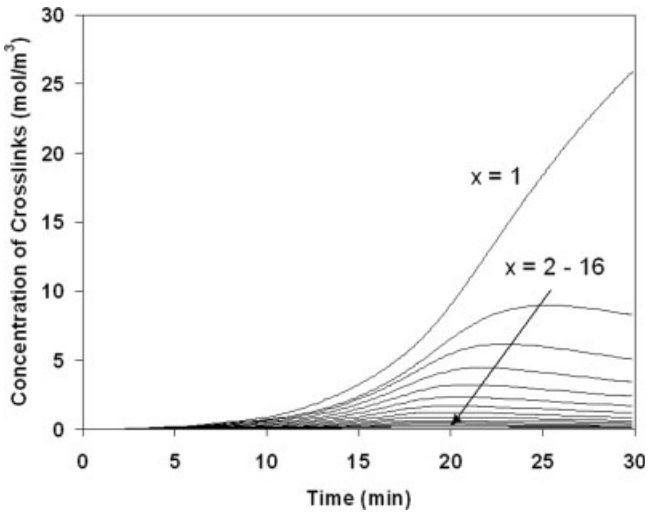

Figure 8 Temporal evolution of mono- ($x = 1$), di- ($x = 2$), and polysulfidic ($x = 3 - 16$) crosslinks for pure NR vulcanization compound at 160°C.

form with relatively lower rate than di- and polysulfidic crosslinks, and only later, as the effect of crosslink desulfuration becomes more distinctive, their concentration exceeds the concentration of other polysulfidic crosslinks, while, as predicted by the present kinetic model, monosulfidic crosslinks are produced with equal (initial stage) if not even higher rate than polysulfidic crosslinks (Fig. 8). While longer crosslinks degrade and desulfurate earlier, the concentration of monosulfidic crosslinks rises steadily as vulcanization proceeds with the overall concentration of crosslinks, also increasing over time until degradation and desulfuration exceed crosslinking in the over-cure region. This of course is conditioned by the temperature of vulcanization. Crosslink formation prediction by our model and its discrepancies from the prediction by Ghosh et al.[3] are attributed to elevated temperature of vulcanization (140–190°C in comparison with the conventional vulcanization at lower temperatures), utilization of two accelerators along with the newly constituted model, which includes a distinction between reactions of species with different numbers of sulfur atoms in the polysulfidic chain.

TABLE VI
Standard Deviations for Estimated Parameters

Kinetic constant	k ($m^3\ mol^{-1}\ s^{-1}$) or (s^{-1})	σ ($m^3\ mol^{-1}\ s^{-1}$) or (s^{-1})
k_{TBBS}	8.95×10^{-6}	1.40×10^{-8}
$k_{TBBS\text{-}MBT}$	5.32×10^{-2}	1.46×10^{-4}
k_{RET}	5.07×10^{-3}	3.06×10^{-5}
k_{CDB}	7.01×10^{-3}	1.06×10^{-5}
k_B	1.08	1.49×10^{-2}
$k_{A\text{-}A}$	7.32	1.28×10^{-2}
$k_{A\text{-}R}$	8.20	1.15×10^{-2}
k_{Vu}	3.98×10^{-1}	1.85×10^{-3}
$k_{B\text{-}R}$	3.84×10^{1}	1.04×10^{-1}
k_{DEG}	4.60×10^{-2}	1.90×10^{-4}
$k_{E\text{-}S}$	3.17	1.59×10^{-2}
$k_{E\text{-}E}$	2.93×10^{-1}	2.32×10^{-2}

The results showed a good correlation between the estimated model parameters for all experiments.[24] An example of the parameter standard deviations for vulcanization of a pure NR compound at 160°C is shown in Table VI.

It may be observed from Figure 9 that the storage modulus rises faster, with increasing set temperature, and at 140°C there is practically no rise in the modulus within 30 min of vulcanization, implying that vulcanization reaction rates are relatively low at this temperature, resulting in long induction times, slow initial descent, and consequentially steady rise of the modulus. However, when vulcanization is conducted at higher temperatures, for example 180°C and 190°C, there are more similarities in the initial curve shape, meaning comparable rise times and induction periods.

It was investigated how the weight ratio of BR and NR in the vulcanization formulation affects the main reactions responsible for product properties. Figure 10 shows the dependence of activation energies on the BR weight fraction. All activation energies rise as the percentage of BR increases, the difference between pure BR and pure NR being most apparent for R. 7, that is, the reaction between the A_X molecule and rubber. Since steric hindrance is greater in polyisoprene chains, one might expect consequentially slower reactions but apparently the influence of the initial polymer chain formation and the methyl group in NR favors reactions between A_X, B_X, B^*_X, and the rubber network. This, however, also has unwanted consequences, as degradation reactions follow the same principle resulting in a higher rate of reversion, represented by the activation energy for R. 10, which also increases as the

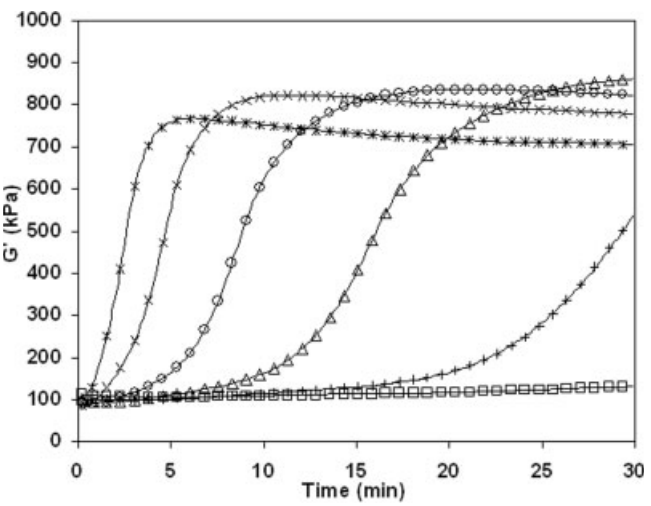

Figure 9 Influence of temperature on vulcanization of BR: (–) vulcanization model; (□) 140°C; (+) 150°C; (△) 160°C; (○) 170°C; (×) 180°C; and (*) 190°C.

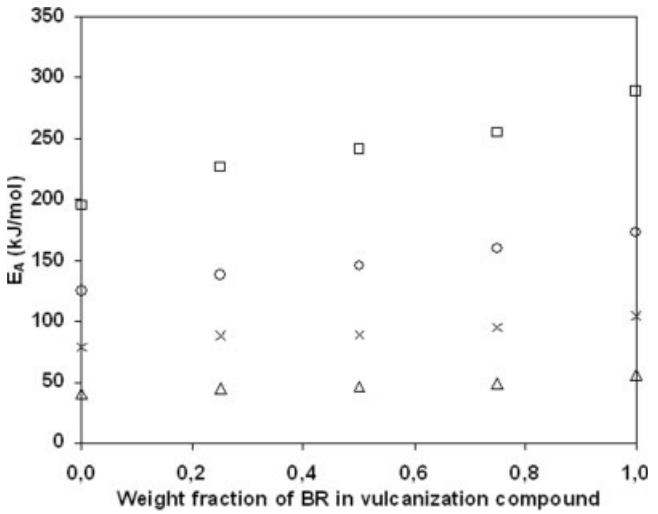

Figure 10 Influence of the weight fraction of butadiene rubber in the vulcanization compound on activation energies of key reactions in Table II: (□) R. 7; (△) R. 8; (×) R. 9; and (○) R. 10.

fraction of BR rises. Considering Figure 10, there are no minima of activation energies for R. 7–R. 9 or maximum of activation energy for R. 10 observed, which would be favorable, if one wanted to choose the optimum constitution of the vulcanization compound for fastest crosslinking and lowest extent of reversion.

CONCLUSIONS

A mechanistic approach was used to model accelerated sulfur vulcanization of different BR/NR blends with two accelerators added to the initial compound. Energy balance and rheological relations were used to thoroughly describe the induction, the cure, and the over-cure period. Molecular modeling was also used to make a distinction between reaction rates of chemically similar species which were previously treated in a lumped fashion.

The reaction scheme, which was a preliminary to differential component mass balances of various species, was upgraded with addition of reactions of both accelerators, and their chemistry and kinetics studied separately using FTIR spectrometry. The best or at least one of the best possible mechanisms for each reaction was considered.

G' changes were confirmed during the vulcanization process because of two contributions, that is, its initial decrease because of increasing compound temperature and later G' rise during the crosslink formation. Two separate experiments with and without added sulfur to the vulcanization compound imply that the modulus minimum is reached at the same time. Later, however, G' of the compound with added sulfur rises steeply whereas G' of the one without added sulfur does not increase much. Moreover, the model predicts that the temperature of the sample will reach the RPA set temperature at practically the same time when G' minimum is reached, meaning that minimal G' during vulcanization and G' when the desired temperature is reached, coincide. An upgraded expression for G' was then used to quantitatively describe both the induction period where the heat transfer regime is determining for G' behavior, and the cure with the postcure region, where the kinetics are determining for its increase.

References

1. Akiba, M.; Hashim, A. S. Prog Polym Sci 1997, 22, 475.
2. Aprem, A. S.; Joseph, K.; Thomas, S. Rubber Chem Technol 2005, 78, 458.
3. Ghosh, P.; Katare, S.; Patkar, P. Rubber Chem Technol 2003, 76, 592.
4. Koenig, J. L. Accounts Chem Res 1999, 32, 1.
5. Piloyan, G. O.; Ryabchikov, I. D.; Novikova, O. S. Nature 1966, 212, 1229.
6. Kamal, M. R.; Sourour, S. Polym Eng Sci 1973, 13, 59.
7. Isayev, A. I.; Deng, J. S. Rubber Chem Technol 1988, 61, 340.
8. Coran, A. Y. Rubber Chem Technol 1964, 37, 689.
9. Ding, R.; Leonov, A. I.; Coran, A. Y. Rubber Chem Technol 1996, 69, 81.
10. Ding, R.; Leonov, A. I. J Appl Polym Sci 1996, 61, 455.
11. Deiber, J. A.; Bortolozzi, R. A.; Pierotti, M. B. J Appl Polym Sci 1995, 56, 967.
12. Deiber, J. A.; Bortolozzi, R. A. J Elast Plast 1995, 27, 329.
13. American Society For Testing Materials. ASTM D 6204. In Annual Book of ASTM Standards. 2002.
14. American Society For Testing Materials. ASTM D 6601. In Annual Book of ASTM Standards. 2003.
15. Bandrup, J.; Immergut, E. H.; Polymer Handbook; Wiley Interscience: New York, 1975.
16. ATHAS Data Bank; Available at http://www.prz.rzeszow.pl/athas/databank/list1.html. Accessed Dec 2005.
17. Coran, A. Y. Rubber Chem Technol 1964, 37, 679.
18. Krejsa, M. R.; Koenig, J. L.; Sullivan, A. B. Rubber Chem Technol 1994, 67, 348.
19. Eirich, F. R. Science and Technology of Rubber; Academic Press: New York, 1978.
20. Coran, A. Y. Chemtech 1983, 13, 106.
21. Fairbrother, F.; Gee, G.; Merrall, G. T. J Polym Sci 1955, 16, 459.
22. Smith, B. C. Infrared Spectral Interpretation; CRC Press: Boca Raton, FL, 1999.
23. Flory, P. J. Principles of Polymer Chemistry; Cornell University Press: Ithaca, NY, 1953.
24. Numerical Algorithms Group, Available at http://www.nag.co.uk/numeric/cl/manual/html/CLlibrarymanual.asp. Accessed Dec 2005